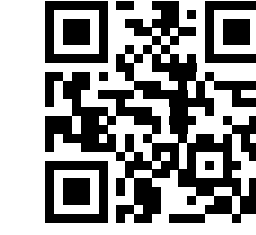


Search for diboson resonance production in the $llqq$ final state using 20.3 fb^{-1} of $\sqrt{s} = 8 \text{ TeV}$ data at ATLAS



Overview

- Heavy diboson resonances are a general test of BSM physics at the TeV scale.
- Benchmark models:
 - Kaluza-Klein Bulk RS graviton (G^*) with $\kappa / m_{\text{Planck}} = 1.0$ [1]
 - Additional vector boson from the extended gauge model (W') with coupling $c = 1$ [2]
- Update to the previous 8 TeV, 7 fb^{-1} analysis. [3]
- The semileptonic channel benefits from a cleaner signal than fully hadronic and higher statistics than fully leptonic.
- High resonance mass leads to boosted bosons and difficult to resolve decay products.
- Split the signal region into three orthogonal regions to optimise sensitivity over a wide mass range.
- Set limits using a profile likelihood simultaneously over all signal regions.

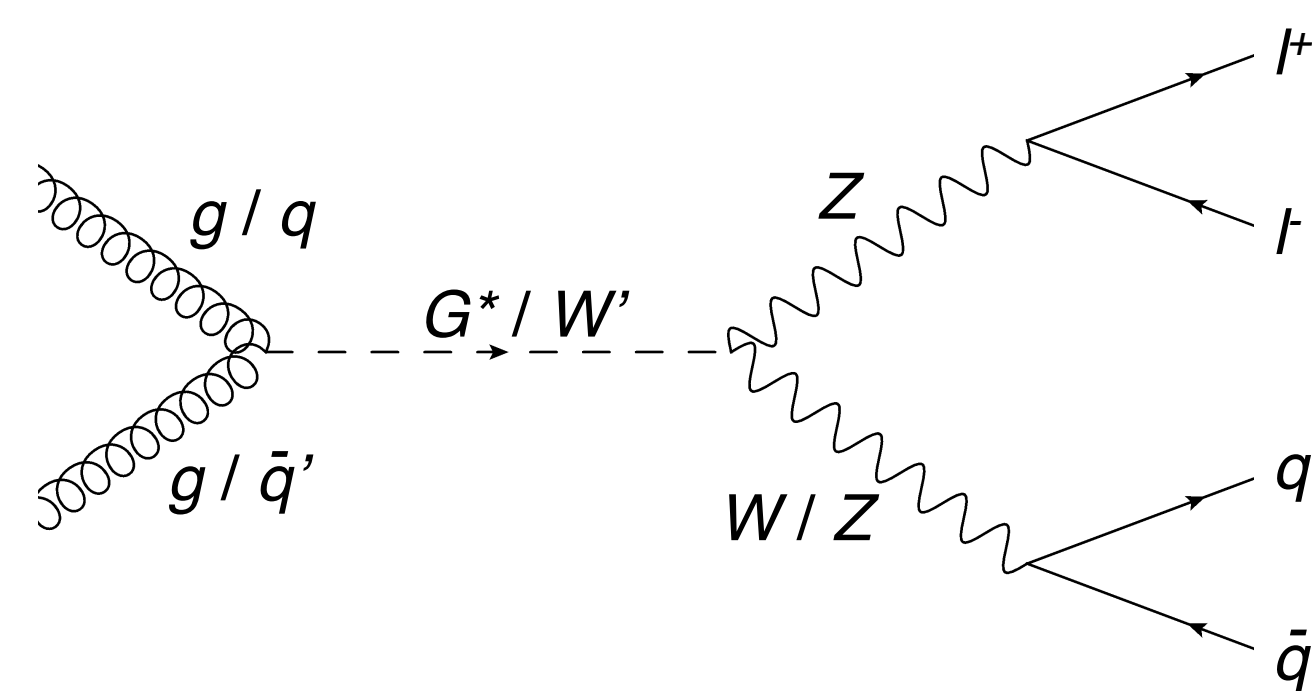


Figure 1. Feynman diagram of the s-channel production of G^* and W' . l refers to either electron or muon.

Boosted Bosons

- High resonance mass leads to boosted bosons.
- Decay products approach each other and become difficult to resolve.
- Substructure variables used to tag large jets as originating from a boson.
- Replace the standard lepton isolation criteria with dilepton isolation criteria.

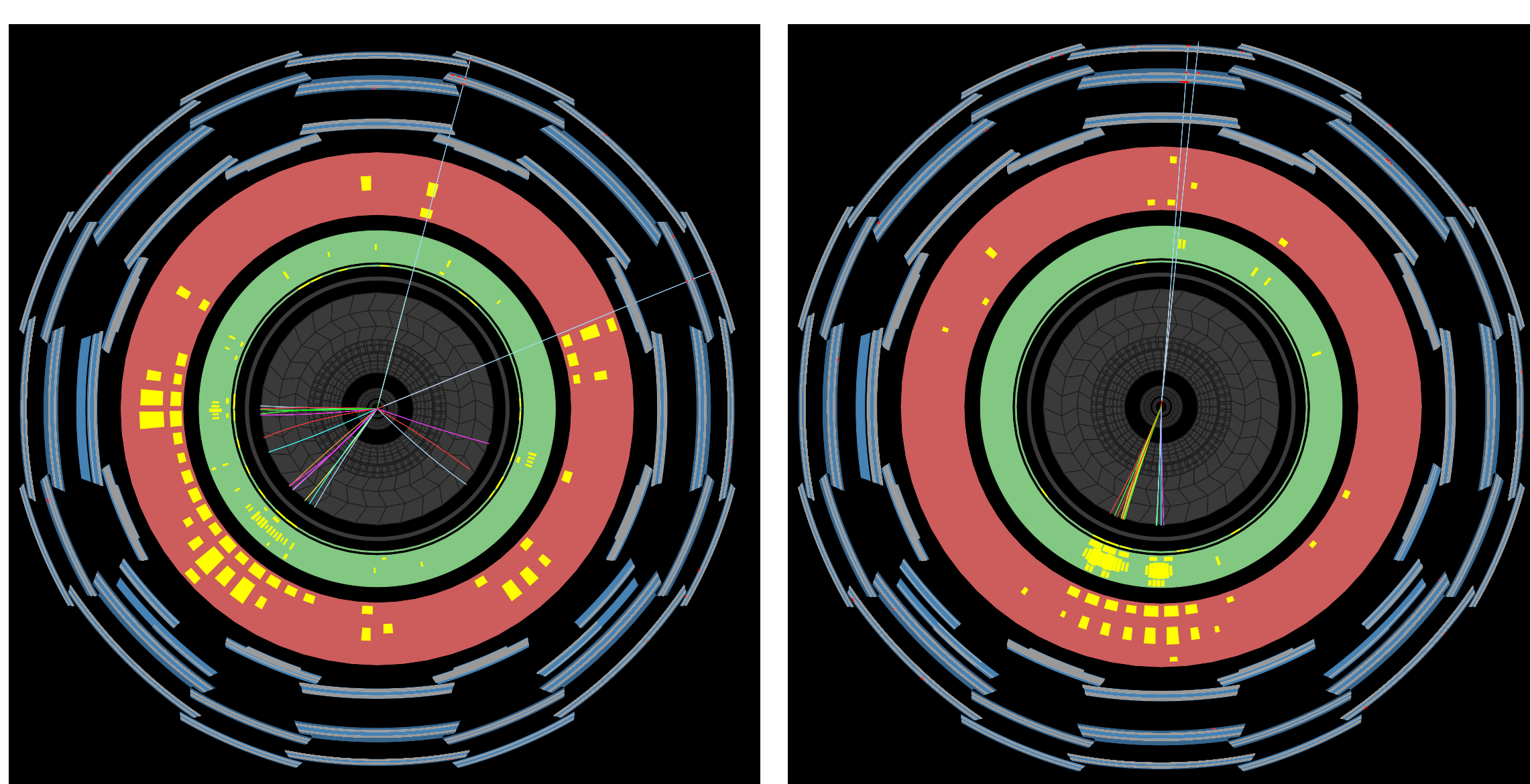


Figure 2. Resolved (left) and merged (right) muon channel signal region event displays, demonstrating the reduced separation of leptons and the merging of the two hadronic jets originating from the boosted bosons.

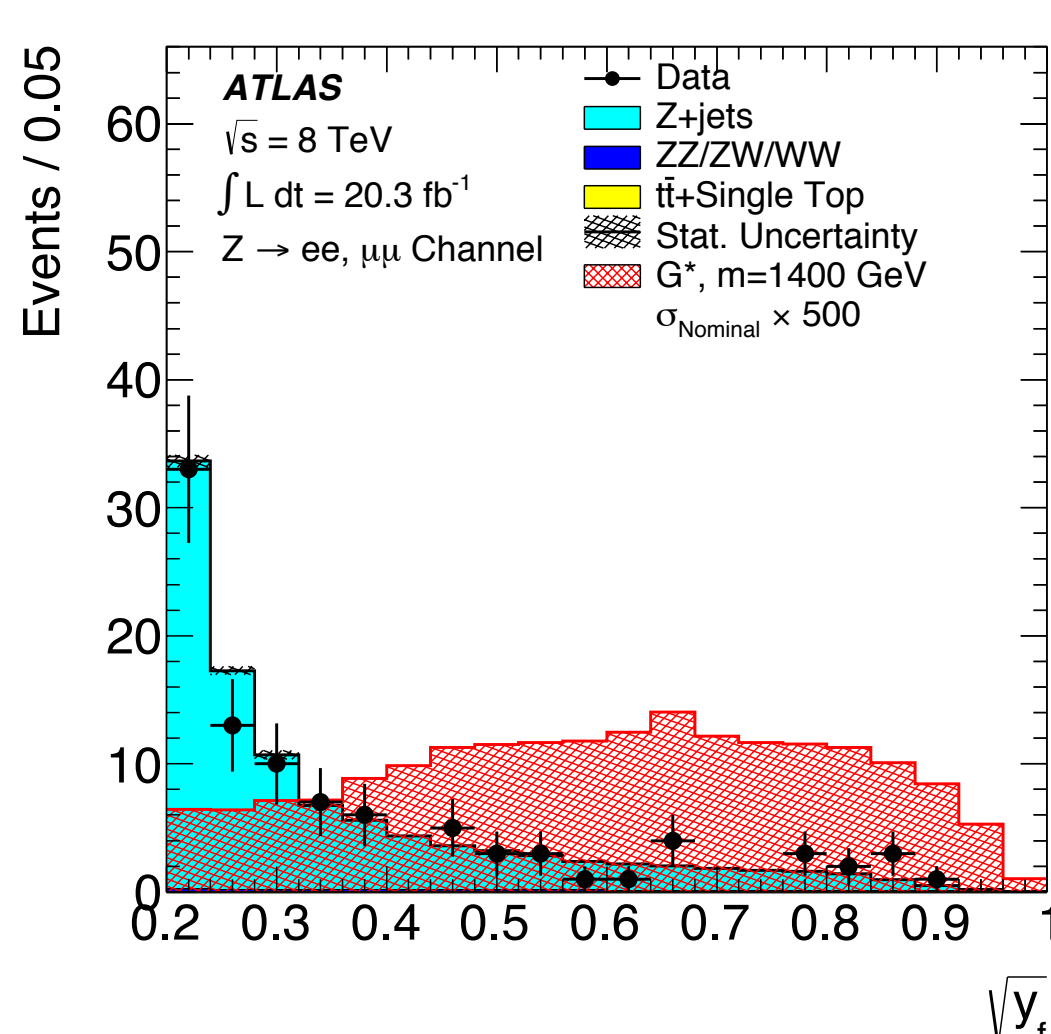


Figure 3. Comparison of data and Monte Carlo of the momentum balance [4] substructure boson tagging variable.

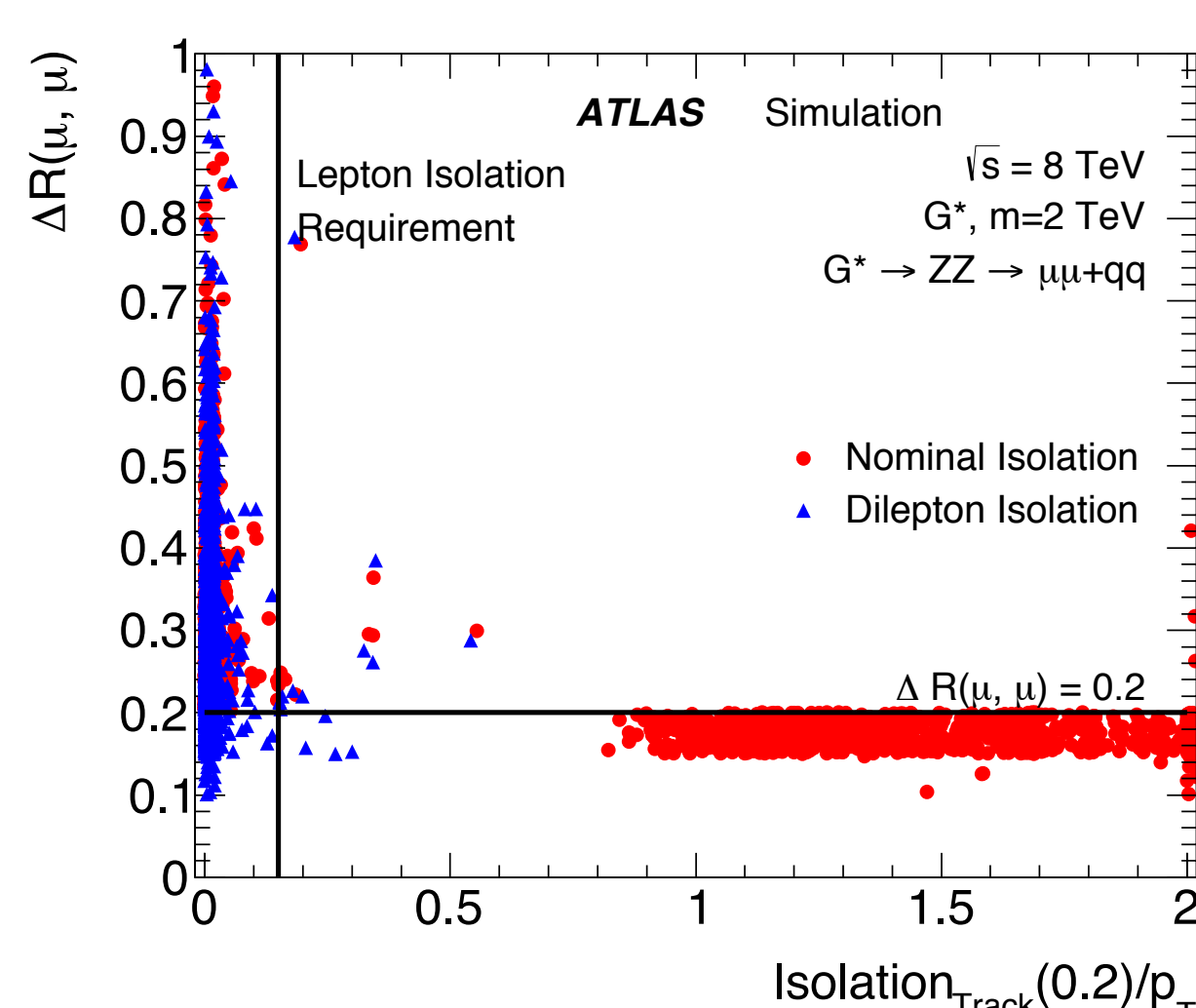


Figure 4. Comparison of standard lepton and dilepton isolation criteria for muons.

Selection Regions

- Divide the signal region into three orthogonal regions to optimise sensitivity across a large mass range.
- Each of these is subsequently divided into electron and muon channels.
- Z + jets is the dominant background in all regions.
- Dominant uncertainty comes from ISR/FSR modeling and is approximately 5%.

Low Resolved Region	High Resolved Region	Merged Region
$p_T(l) > 100 \text{ GeV}$	$p_T(l) > 250 \text{ GeV}$	$p_T(l) > 400 \text{ GeV}$
$p_T(j) > 100 \text{ GeV}$	$p_T(j) > 250 \text{ GeV}$	$p_T(j) > 400 \text{ GeV}$
$70 \text{ GeV} < M(jj) < 110 \text{ GeV}$	$70 \text{ GeV} < M(jj) < 110 \text{ GeV}$	$70 \text{ GeV} < M(J) < 110 \text{ GeV}$
		$\sqrt{y_r(J)} > 0.45$

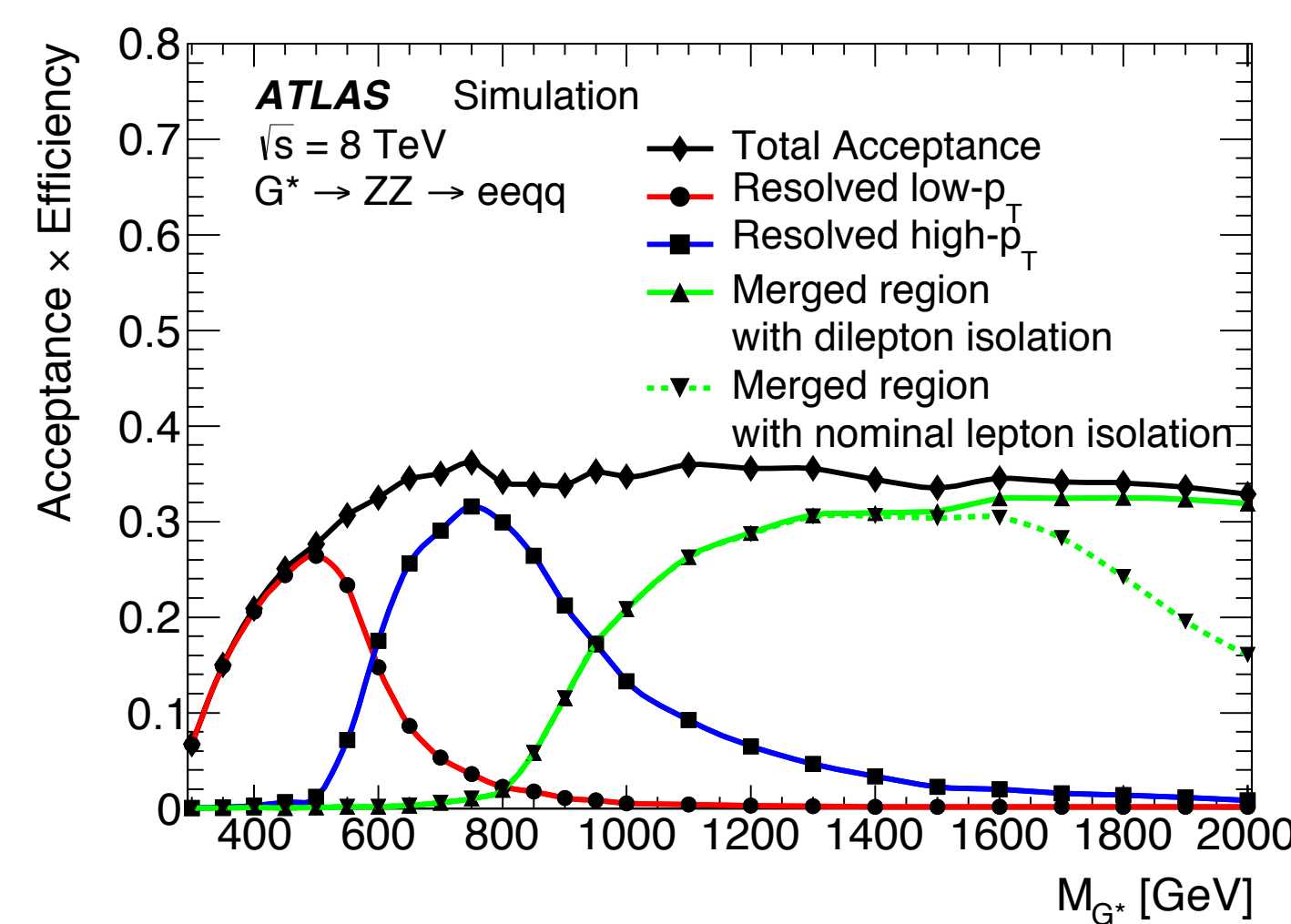


Figure 5. The signal acceptance as a function of G^* mass for the three regions and their combination in the electron channel.

Results

- No large excesses are observed and mass constraints are set
- $M_{G^*} > 740 \text{ GeV}$
 $M_{W'} > 1,590 \text{ GeV}$

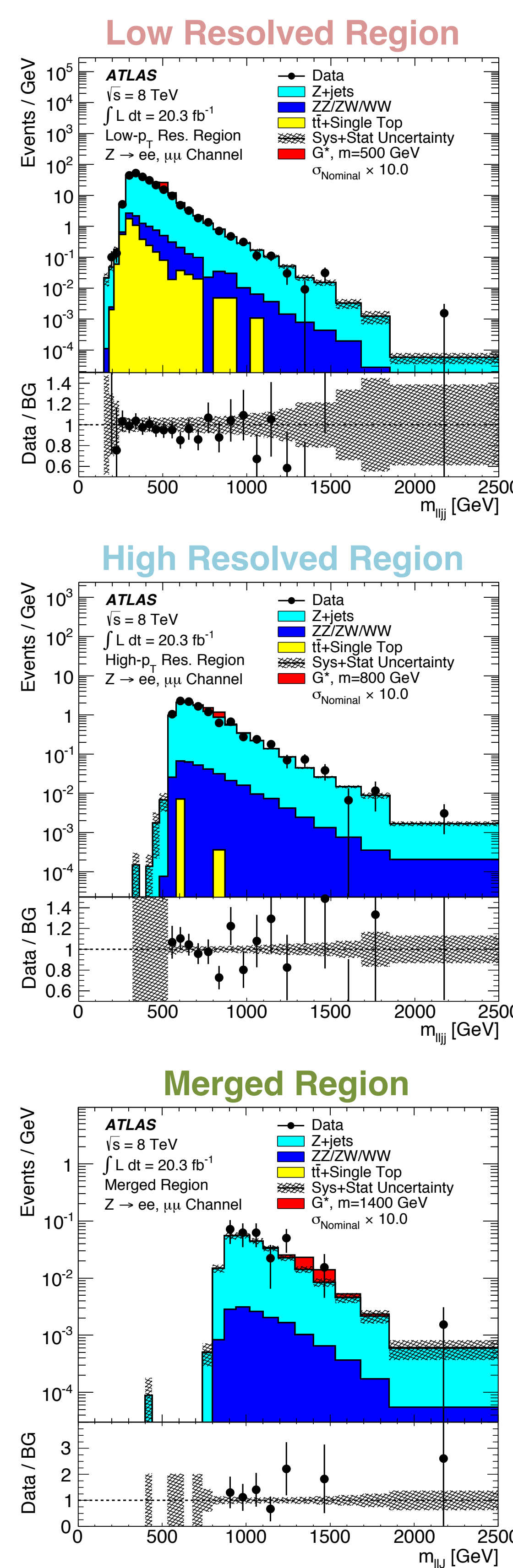


Figure 6. Comparison of data to Monte Carlo background for the reconstructed $lljj$ or llJ mass in the low resolved (top), high resolved (middle) and merged (bottom) region.

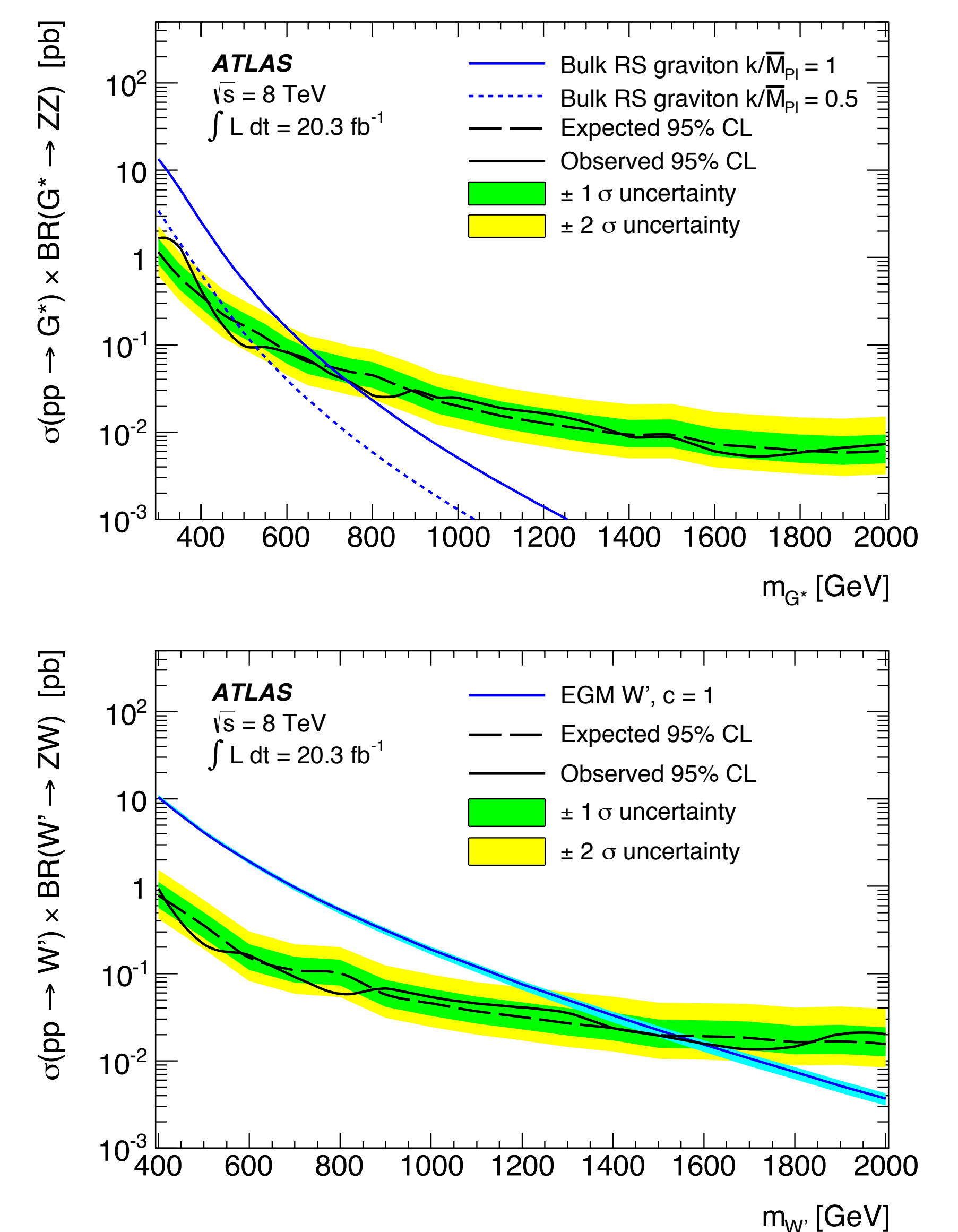


Figure 7. The 95% CL upper limits on the cross section times branching fraction as a function of the resonance pole mass for the G^* (top) and W' (bottom).

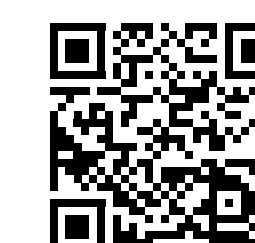
[1] K. Agashe et al., Phys. Rev. D 76, 036006 (2007)



[3] ATLAS Collaboration, ATLAS-CONF-2012-150



[2] G. Altarelli, B. Mele, and M. Ruiz-Altaba, Z. Phys. C 45, 109 (1989)



[4] ATLAS Collaboration, ATL-PHYS-PUB-2014-004

